



HAL
open science

Pore connectivity, permeability, and electrical formation factor: A new model and comparison to experimental data

Y. Bernabé, M. Zamora, M. Li, A. Maineult, Y. B. Tang

► **To cite this version:**

Y. Bernabé, M. Zamora, M. Li, A. Maineult, Y. B. Tang. Pore connectivity, permeability, and electrical formation factor: A new model and comparison to experimental data. *Journal of Geophysical Research: Solid Earth*, 2011, 116, <10.1029/2011JB008543>. <insu-03606430>

HAL Id: insu-03606430

<https://insu.hal.science/insu-03606430v1>

Submitted on 12 Mar 2022

HAL is a multi-disciplinary open access archive for the deposit and dissemination of scientific research documents, whether they are published or not. The documents may come from teaching and research institutions in France or abroad, or from public or private research centers.

L'archive ouverte pluridisciplinaire **HAL**, est destinée au dépôt et à la diffusion de documents scientifiques de niveau recherche, publiés ou non, émanant des établissements d'enseignement et de recherche français ou étrangers, des laboratoires publics ou privés.



Copyright - All rights reserved

Pore connectivity, permeability, and electrical formation factor: A new model and comparison to experimental data

Y. Bernabé,¹ M. Zamora,² M. Li,³ A. Maineuil,² and Y. B. Tang³

Received 23 May 2011; revised 1 August 2011; accepted 31 August 2011; published 12 November 2011.

[1] This paper is a follow up on Bernabé et al.'s (2010) study of the effect of pore connectivity and pore size heterogeneity on permeability. In the permeability model initially proposed, pore connectivity was characterized by means of the average coordination number z , a parameter rarely included in experimental investigations of the transport properties and microstructure of porous rocks. Obviously, lack of information on z makes it difficult to apply the model. One way around this problem is to eliminate z from the model by introducing the resistivity formation factor, an approach previously used by Paterson (1983), Walsh and Brace (1984), and many others. Using the network simulation approach of Bernabé et al. (2010), we extended the model to include the electrical formation factor. The new joint permeability-formation factor model consists of three equations, the first two expressing the relation of permeability and formation factor to z and the last one, obtained by elimination of z , linking permeability and formation with each other. We satisfactorily tested the model by comparison with published experimental data on a variety of granular materials and rocks. Furthermore, we show that, although our model does not explicitly include porosity, it is consistent with Archie's law.

Citation: Bernabé, Y., M. Zamora, M. Li, A. Maineuil, and Y. B. Tang (2011), Pore connectivity, permeability, and electrical formation factor: A new model and comparison to experimental data, *J. Geophys. Res.*, 116, B11204, doi:10.1029/2011JB008543.

1. Introduction

[2] Owing to mechanical and/or chemical interactions with rocks, interstitial fluids are central to many geologic processes as well as geotechnical applications such as oil and gas production or geothermal energy recovery. Hence, we need the best possible understanding of the material property controlling interstitial fluid motion: permeability (denoted k and measured in 10^{-12} m² or D). However, k is particularly challenging to model. In the Earth, it varies well over 11 orders of magnitude [e.g., Brace, 1980]. Even for a single rock type, the range of variation of k can cover many orders of magnitude. One reason for this extreme variability is that permeability strongly depends on pore connectivity [e.g., Guéguen and Dienes, 1989] and all degrees of connectivity exist in rocks. For example, consider enormously porous but impermeable pumice stones (zero connectivity) and highly permeable sand beds (very high connectivity).

[3] Bernabé, Li, and Maineuil (BLM) recently proposed a permeability model focused on quantifying the effect of

connectivity [Bernabé et al., 2010]. In this model, pore connectivity is measured by means of the average coordination number z (i.e., mean number of conduits or throats attached to a nodal pore). Using network simulations, BLM found that the permeability of networks is well approximated by the power law, $k = \kappa (z - z_c)^\beta$, where z_c is the critical coordination number at the percolation threshold ($z_c = 1.5$ for three-dimensional pipe networks), and where the exponent β and pre-factor κ are functions of the width of the pore radius distribution, or, in other words, of pore size heterogeneity. One important result is that this power law holds in the entire range of z , except very near the percolation threshold z_c . Thus, the model should be applicable to rocks with widely different permeabilities. Unfortunately, z is not a parameter frequently measured in rocks. In fact, BLM were able to test their model on only one rock, Fontainebleau sandstone. One way to enhance the applicability of the model is to introduce the resistivity formation factor F , an approach previously used by Paterson [1983], Walsh and Brace [1984], and many others to get rid of tortuosity, a poorly constrained parameter that is impossible to measure independently. The relation of F to porosity (i.e., Archie's law) was used by Revil and Cathles [1999] to construct a model of the permeability of sand-clay mixtures (see also Glover [2009] for a discussion of Archie's law in terms of pore connectivity). F is measurable in any porous rock but its simple, commonly applied definition as the ratio of the rock electrical resistivity to the fluid resistivity is only valid in electrically uncharged materials (note that

¹Earth, Atmospheric and Planetary Sciences Department, Massachusetts Institute of Technology, Cambridge, Massachusetts, USA.

²Institut de Physique du Globe de Paris, Sorbonne Paris Cité, Université Paris Diderot, Paris, France.

³State Key Laboratory of Oil and Gas Reservoir Geology and Exploitation, Southwest Petroleum University, Chengdu, China.

the formation factor concept only applies to rocks that do not contain electrically conductive mineral components). In general, the pore walls in contact with an ionic solution are electrically charged and a more complex definition must be used [e.g., *Revil and Glover*, 1997, 1998; *Revil*, 1999, 2002]. The model derived in section 3 requires F to be properly measured, using a range of saturating fluids with different saline concentrations and a nonlinear inversion method such as that of *Bernard et al.* [2007]. However, accurate values of F can be obtained with a single saturating fluid in materials with low surface conduction (e.g., clayless sands), provided the saline concentration used is sufficiently high (this condition was met for essentially all the experimental data used in section 4).

[4] In this paper, we extend the BLM network simulations to electrical conduction through saturated porous media. The main result is that, just like permeability, the inverse formation factor can be modeled by a power law function, $1/F \propto (z-z_c)^\gamma$. We then derive a joint model of k and F , consisting of three equations, the first two expressing the relation of k and $1/F$ to $z-z_c$ and the last one, obtained by elimination of $z-z_c$, linking k to $1/F$. We test the model against experimental data on several materials, for which the model parameters either were actually measured or could be reliably inferred. Finally, we discuss some features of the model, in particular its connection to Archie's law.

2. Network Simulations of Electrical Conduction Through Saturated Porous Media

2.1. Background

[5] The main concept used by BLM is that permeability is the product of a squared length scale L^2 by a dimensionless, scale-invariant function H [*Berryman*, 1992a, 1992b, 1993]. Note that here "scale-invariant" means invariant under application of a transform such that the physical distance separating any pair of points in the medium is scaled by a constant factor. This term should not be confused with "zoom-invariant," an expression referring to fractal structures. In order to separate scale-variant and scale-invariant effects, BLM defined L as a purely geometric quantity. Following a long tradition in rock physics, they used the hydraulic radius r_H (i.e., $r_H = 2V_p/A_p$, where V_p is the pore volume and A_p the surface area of the pore-solid interface; note that the hydraulic radius is sometimes defined as $V_p/A_p = r_H/2$). Since it is impossible to list all possible scale-invariant effects, BLM limited their analysis to the effect of connectivity (measured by the mean coordination number z) and pore size heterogeneity (measured by σ_r , the standard deviation of the pore radii normalized to the mean pore radius). These two effects were investigated using numerical simulations of fluid flow through networks of pipes. In order to isolate the function H , BLM constructed network realizations with a fixed value of the hydraulic radius, namely, $r_H = 40 \mu\text{m}$.

[6] The BLM network simulation approach was largely inspired by early works on percolation theory. The main goal was to search for "universal" relationships among the network parameters (i.e., relationships valid for all lattice types [e.g., *Stauffer and Aharony*, 1992; *Sahimi*, 1995, and references therein]). Indeed, although networks of pipes

cannot be taken as realistic representations of porous rocks, "universal" network properties (i.e., independent of lattice type) can reasonably be generalized to real porous rocks, especially to those in which a medial axis can be determined (i.e., reduction of the pore space to its underlying topological skeleton [*Thovert et al.*, 2001; *Spanne et al.*, 1994; *Lindquist et al.*, 1996; *Baldwin et al.*, 1996; *Fredrich and Lindquist*, 1997; *Lindquist and Venkatarangan*, 1999; *Fredrich*, 1999; *Lindquist et al.*, 2000; *Petford et al.*, 2001; *Sok et al.*, 2002]). For this purpose, BLM simulated fluid flow through three different, three-dimensional, regular lattices, namely, simple cubic (SC), body-centered cubic (BCC), and face-centered cubic (FCC). For each value of σ_r and z , porosity ϕ and permeability k were measured. In order to identify "universal" relationships, BLM considered various combinations of ϕ and k (e.g., k/ϕ , k , $k\phi$, and so forth) and plotted the corresponding numerical results for each value of σ_r against $z-z_c$ in log-log scale. It turns out that the combination of ϕ and k producing the straightest lines with least scatter, was simply k alone (note that, for two-dimensional lattices, the product $k\phi$ was the optimal combination). BLM concluded that k obeys the following "universal" power law:

$$k = \frac{w_k \pi}{8} \left(\frac{r_H}{l} \right)^2 (z - z_c)^\beta r_H^2, \quad (1)$$

where w_k and β depend on σ_r (the factor $\pi/8(r_H/l)^2$ in equation (1) is a consequence of Poiseuille formula).

[7] In the present paper, the BLM method is applied to electrical conduction through networks of infinitely resistive pipes saturated with an electrolyte of conductivity σ_f . Surface conduction can also be accounted for [e.g., *Bernabé*, 1998]. However, since our main purpose is to investigate F , we simply assumed that surface conduction was absent in the networks. In this case, F is equal to the ratio of the fluid conductivity to the calculated network conductivity σ (i.e., $F = \sigma_f/\sigma$).

2.2. Numerical Procedures

[8] In the BLM network simulations, pore size heterogeneity was generated by randomly assigning the radius r_i of each pipe i in the network. The pipe radii were assumed to be independent stochastic variables, obeying the same probability density function (thus producing nominally isotropic network realizations). Since strongly skewed pore radii distributions are usually observed in rocks [e.g., *Fredrich and Lindquist*, 1997; *Lindquist et al.*, 2000], BLM used log-uniform distributions with different values of σ_r , the standard deviation normalized to the mean radius. The pore radii distributions used by BLM were also designed to produce a constant value $r_H = 40 \mu\text{m}$ in all network realizations (the specific rules used by BLM can be found in the work of *Bernabé et al.* [2010]). Since k is much less affected by the variations of pore length than of pore radius, BLM restricted the simulations to regular lattices, for which the pipe length l is a constant ($l = 300 \mu\text{m}$ was used in all network realizations). Note that σ_r is equivalently defined as the normalized standard deviation of the hydraulic radii of individual pores, a quantity that can be measured in real materials using quantitative two- or three-dimensional

microstructure analysis (e.g., stereological measurements of local pore volume and surface area).

[9] Variations in coordination number were produced by randomly selecting a number of pipes according to a probability $1-p$ and assigning them a radius equal to zero. It is important to note that the critical value p_c of the occupancy probability p at the percolation threshold is lattice-specific (i.e., not “universal”). For example, $p_c = 0.249, 0.180,$ and 0.120 have been determined for the SC, BCC, and FCC networks, respectively [e.g., *Sahimi*, 1995]. On the other hand, the critical mean coordination number z_c is very nearly “universal” ($z_c \approx 2$ and 1.5 , in two- and three-dimensional lattices, respectively [e.g., *Sahimi*, 1995]). The “universality” of z_c is a crucial property that may explain the “universality” of the $k \propto (z-z_c)^\beta$ power laws observed by BLM.

[10] In order to simulate fluid flow through a network realization, periodic boundary conditions were applied and the values of fluid pressure at the nodes were calculated by solving Kirchoff laws (see *Bernabé et al.* [2010, and references therein] for more details). For an individual pipe i , the volumetric fluid flux $q_i^{(h)}$ is given by

$$q_i^{(h)} = -g_i^{(h)} \frac{\Delta p_i}{\eta}, \quad (2)$$

where $g_i^{(h)}$ is the hydraulic conductance, Δp_i is the pore pressure difference across the pipe, and η is the fluid viscosity. For pipes with circular cross-sections, Poiseuille formula yields

$$g_i^{(h)} = \frac{\pi r_i^4}{8l}. \quad (3)$$

By definition, the local hydraulic radius is equal to r_i , the pipe radius. In the case of pipes with elliptic cross-sections, this expression becomes

$$g_i^{(h)} = \frac{\pi a_i^3 b_i^3}{4l(a_i^2 + b_i^2)}, \quad (4)$$

where a_i and b_i are the major and minor dimensions, respectively. The local hydraulic radius (simply denoted r_i) can be obtained from the cross-sectional area ($A_i = \pi a_i b_i$) and perimeter ($P_i \approx \pi [3(a_i + b_i) - (3a_i^2 + 10a_i b_i + 3b_i^2)^{1/2}]$, from *Ramanujan* formula). Equation (4) can then be rewritten as

$$g_i^{(h)} = \frac{\pi r_i^4 [3(1 + \varepsilon) - \sqrt{3\varepsilon^2 + 10\varepsilon + 3}]^4}{64l\varepsilon(1 + \varepsilon^2)} = f(\varepsilon) \frac{\pi r_i^4}{8l}, \quad (5)$$

where $\varepsilon = b_i/a_i$ is the cross-section aspect ratio. BLM only considered pipes with circular cross-sections (i.e., $\varepsilon = 1$). But the permeability k of any of their network realizations can be transformed into that of a network of elliptic pipes with constant aspect ratio ε by multiplying k by $f(\varepsilon)$ as defined in equation (5). It is, in principle, possible to consider the more general case of a distribution of aspect ratios but this will lead to an even more complex model, in which at least one additional heterogeneity parameter must be introduced. We applied the BLM numerical method (see

Bernabé et al. [2010] for the details) to electrical conduction by replacing equations (2), (3), and (5), respectively by

$$q_i^{(e)} = -g_i^{(e)} \Delta u_i, \quad (6)$$

$$g_i^{(e)} = \sigma_f \frac{\pi r_i^2}{l}, \quad (7)$$

$$g_i^{(e)} = \sigma_f \frac{\pi r_i^2 [3(1 + \varepsilon) - \sqrt{3\varepsilon^2 + 10\varepsilon + 3}]^2}{4l\varepsilon}, \quad (8)$$

where $q_i^{(e)}$ is the electric current, $g_i^{(e)}$ is the electrical conductance, and Δu_i is the electrical potential difference. As in the BLM study, we used $15 \times 15 \times 15$, $12 \times 12 \times 12$, and $14 \times 14 \times 14$ networks for SC, FCC, and BCC, respectively, and the numerical results reported in the next sections are ensemble averages over at least 200 realizations. The statistical relative fluctuations of $1/F$ were much lower than 1% in general (they were always smaller than the fluctuations of k), although relative fluctuations as large as 20% did occur for highly heterogeneous networks near the percolation threshold (i.e., $\sigma_r = 1.05$ and $z-z_c < 0.4$). However, large uncertainties near the percolation threshold are not really a problem because the vicinity of z_c (i.e., $z-z_c < 0.4$) is excluded from this study. Indeed, in a very small domain near the percolation threshold, the critical power law $1/F \propto (p-p_c)^\nu$ of percolation theory must hold, implying that the power law $1/F \propto (z-z_c)^\gamma$ observed in our simulations should not be valid near z_c .

2.3. Analysis of the Numerical Results

[11] Having performed the network simulations described in the previous section, we followed the BLM analysis and examined the relationships of various combinations of ϕ and $1/F$ to $z-z_c$ and arrived at the same conclusion as for k , namely that $1/F$ obeyed the following “universal” power law (see Figure 1a):

$$1/F = w_F \pi \left(\frac{r_H}{l}\right)^2 (z - z_c)^\gamma, \quad (9)$$

where γ and w_F are functions of σ_r (see Table 1). This result may appear to be a direct consequence of the fact that hydraulic flow and electrical conduction simulation obey the same formal set of linear equations, the only difference being that local hydraulic and electrical conductances are proportional to r_i^4 and r_i^2 , respectively. However, the response to a random distribution of pipe radii is very different in both cases. For example, *David* [1993] showed that the (very complex) spatial distributions of local fluid flow and electrical current in two-dimensional heterogeneous networks were quite dissimilar (in particular, hydraulic and electrical tortuosities were not equal). Similarly, we note here that the exponents β and γ did not take simple values and were not related to each other in any simple way. Combining equations (1) and (9) yields

$$k = \frac{w \pi^{1-\alpha}}{8} \left(\frac{r_H}{l}\right)^{2(1-\alpha)} (1/F)^\alpha r_H^2, \quad (10)$$

where $\alpha = \beta/\gamma$ and $w = w_k w_F^{-\alpha}$. Indeed, plotting k against $1/F$ in log-log scale yields a set of very well defined straight lines

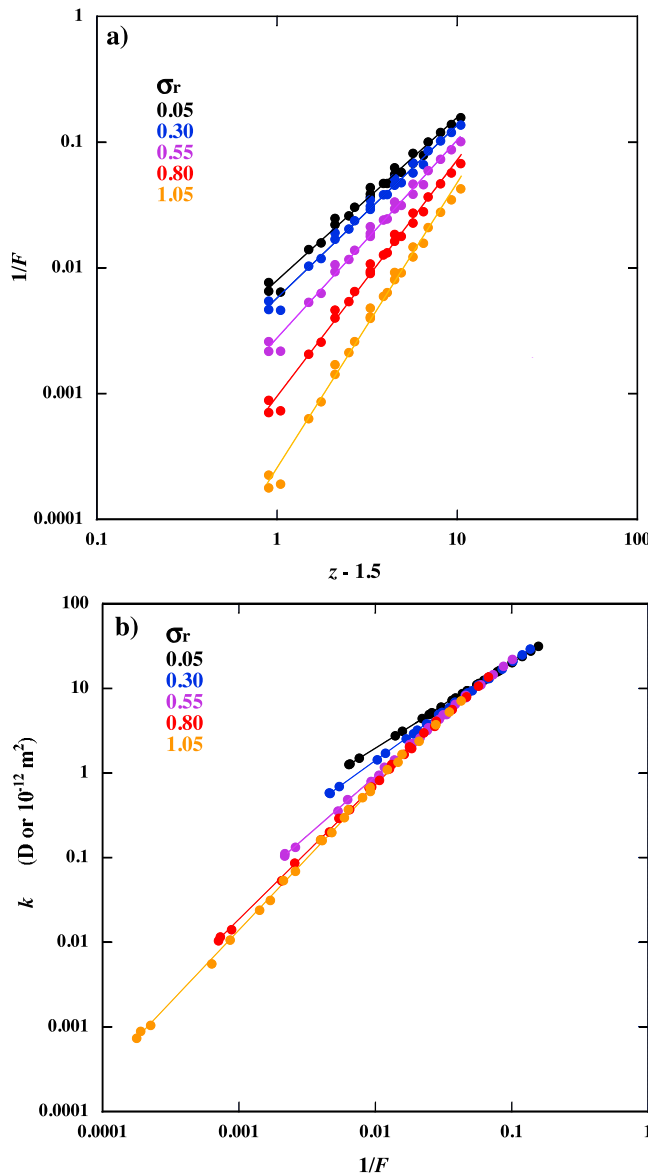


Figure 1. Illustrations of the “universal” power laws satisfied for various values of σ_r (namely, 0.05, 0.30, 0.55, 0.80, and 1.05, indicated in black, blue, purple, red, and orange, respectively) by (a) the inverse formation factor $1/F$ with respect to $z - z_c$, and (b) permeability k as a function of $1/F$. Results obtained using SC, BCC, and FCC lattices are intermixed in the diagram.

(see Figure 1b), with exponents and pre-factors values consistent with the relationships mentioned above (see Table 1).

[12] Notice that the power law lines for different values of σ_r shown in Figure 1b overlap significantly for high values of z and only spread apart in the low z domain. In other words, the relationship between k and $1/F$ is strongly sensitive to pore scale heterogeneity only in poorly connected networks.

3. Inferred Model

[13] Although networks of pipes are not realistic representations of porous rocks, they can provide helpful insight

for identifying “universal” relations such as equations (1), (9), and (10), among the transport properties and microstructure attributes of porous media. These equations can be rewritten as

$$k = C_k \left(\frac{r_H}{l}\right)^2 (z - z_c)^\beta r_H^2, \quad (11)$$

$$1/F = C_F \left(\frac{r_H}{l}\right)^2 (z - z_c)^\gamma, \quad (12)$$

$$k = C \left(\frac{r_H}{l}\right)^{2(1-\alpha)} (1/F)^\alpha r_H^2, \quad (13)$$

where the pre-factors C_k , C_F , and C were explicitly given in the previous sections for pipes with circular cross-sections. In order to simplify our notations, equations (11), (12), and (13) will be hereafter called the kz -, Fz -, and kF -equations, respectively, and the subscripts kz -, Fz -, and kF will be correspondingly applied to quantities related to them. Examining the values given in Table 1, we found that β , γ , $\log_{10}(C_k)$, and $\log_{10}(C_F)$ could be well approximated by second degree polynomials in σ_r . The dependence on ε is easily included using equations (5) and (8). We thus have analytical expressions giving the constants of the model for σ_r varying from 0.1 to 1 and for any value of ε between 0 and 1 (see Appendix A). Note that the formulas in Appendix A expressing the dependence on σ_r were derived empirically. They may have to be modified if another range of σ_r is considered.

[14] In summary, this model contains four scale-invariant parameters: (1) z the mean coordination number, (2) σ_r the normalized standard deviation of the pore hydraulic radii distribution, (3) the ratio r_H/l , and (4) the aspect ratio ε of the pore cross-sections. One scale-invariant parameter notably absent is porosity. Although surprising at first sight, the absence of porosity is not illogical. Indeed, it is well known that poorly connected pores (for example, dead-end pores) can be arbitrarily added to or removed from the pore space without significantly affecting k and F . This precludes the existence of a general ϕ - k relationship [e.g., Bernabé *et al.*, 2003]. It may be noticed that $(r_H/l)^2 = \phi/3\pi$ in a perfectly homogeneous SC network but this expression is not “universal” (i.e., it is different for BCC and FCC networks), implying that the ratio r_H/l cannot be replaced by porosity.

4. Testing the Model: Comparison With Experimental Data

[15] Ideally, testing the model entails selecting a broad variety of rocks, measuring all the needed quantities on each

Table 1. Observed Values of the Exponents and Pre-Factors of the Power Laws of Equations (1), (9), and (10)

σ_r	α	β	γ	w	w_k	w_F
0.05	1.01	1.31	1.29	0.997	0.139	0.143
0.30	1.17	1.60	1.38	0.934	0.0666	0.103
0.55	1.41	2.19	1.57	0.919	0.0139	0.0493
0.80	1.60	2.94	1.87	1.023	0.00169	0.0171
1.05	1.70	3.79	2.26	1.176	0.000137	0.00459

one of them, and comparing the measured values of k and F with those predicted by the model. But this endeavor requires a large amount of time and, although we plan to make the attempt in the future, we decided first to carry out a preliminary assessment of the model using data sets from the literature. One severe problem, however, was that we could not find any instance of a rock or material for which all needed quantities had been measured. As already mentioned, the coordination number z has very rarely been measured to date. Even, a much simpler parameter such as the pore length l is usually not included in microstructure studies. The closest to the ideal we could come up with was Fontainebleau sandstone. But, even in this case, three separate data sets had to be merged, increasing the modeling uncertainty (see section 4.3 and Bernabé *et al.* [2010]). Furthermore, the merged data set still did not include σ_r and ε .

[16] We must therefore devise methods using additional, independent information to estimate the parameters missing in the data sets considered. For example, observed statistics of various microstructural attributes such as pore length or throat size helped constrain σ_r in Fontainebleau sandstone (see section 4.3). Unfortunately, there may still be some very poorly constrained parameters. In such cases, we tried to determine the input values or ranges of input values producing the best fit to the experimental data and verified a posteriori that the optimized parameters were plausible. Note that the optimization scheme had to be applied to the three kz -, Fz -, and kF -equations simultaneously. We performed it on a sample-by-sample basis but, owing to the statistical fluctuations likely to occur among small rock samples, the optimized parameters usually presented significant fluctuations that had to be smoothed out statistically. Given the wide differences in materials and parameters considered in sections 4.1–4.4, we had to use a different treatment in each case (in fact, many different techniques could be used equally well; they should all lead to very similar sets of input parameters).

[17] For the sake of consistency, we used a unique misfit measure to assess the fit quality in all cases. Owing to the large range of permeability covered (see sections 4.1–4.4), we defined the misfit for an individual permeability data point as $x_k = \lvert \log(k_{\text{calculated}}) - \log(k_{\text{measured}}) \rvert$. Notice that using the L1 norm has the advantage of preserving the properties of logs and exponentials to transform products into sums and vice versa. Thus, the above definition is equivalent to stating that the calculated and measured k are in agreement with each other within a factor $\xi_k = \exp[x_k]$. When considering a group of data points, the representative misfit measure and misfit factor are simply given by the arithmetic and geometric averages of the individual x_k 's and ξ_k 's, respectively. Although the range of F in the data sets considered is much smaller than the one covered by k , we used the same definitions of misfit as described above. Finally, to simplify the description of our results, we will hereafter denote x_{kz} , x_{Fz} , x_{kF} , ξ_{kz} , ξ_{Fz} , and ξ_{kF} the misfit measures and misfit factors corresponding to the kz -, Fz -, and kF -equations, respectively.

4.1. Well-Sorted, Unconsolidated Granular Media

[18] We first considered unconsolidated, very well sorted, granular materials. Glover and Walker [2009] and Glover and Déry [2010] packed extremely well sorted glass beads

with a mean grain radius R ranging from 0.5 to 3000 μm . The measured porosity ϕ and formation factor F were nearly constant ($\phi = 39.1 \pm 1.1\%$, $F = 4.1 \pm 0.3$) whereas permeability k increased approximately as R^2 (samples “G” to “M” from Glover and Walker [2009, Table 1] have misprinted permeability values, too high by a factor of 10). Biella and Tabacco [1981] and Biella *et al.* [1983] washed, sieved, and packed natural sands collected from two alluvial deposits. The mean grain radius ranged from 75 to 3575 μm . The sand samples prepared by Biella *et al.* [1983] had $\phi = 39.5 \pm 2.7\%$ and $F = 4.4 \pm 0.3$, and, furthermore showed a weak dependence of ϕ and F with R . These sands were described as consisting of rounded grains, except the sample labeled “a” [Biella *et al.*, 1983, Table 1], which partly contained platy grains. No such description was given in Biella and Tabacco [1981] but micrographs of the sand grains suggest that moderately angular and/or elongated grains were common. In contrast with the sands prepared by Biella *et al.*'s [1983], the Biella and Tabacco's [1981] sands had a rather large porosity and small formation factor ($\phi = 47.9 \pm 1.1\%$, $F = 3.3 \pm 0.2$). Note that Biella and Tabacco [1981] used two different packing procedures, one of which, for unknown reasons, yielded significantly outlying data points in their Figures 6 and 8. These outliers were not included in our analysis. Hereafter, we call Biella 1 the data set containing the data from Biella *et al.* [1983] except sample “a,” which together with the Biella and Tabacco's [1981] data form the Biella 2 data set. The Glover and Walker [2009] and Glover and Déry [2010] data are grouped into the Glover data set.

[19] In order to test our model, we must estimate five parameters, namely, z , l , r_H , σ_r , and ε . We reasoned as follows:

[20] 1. There are no reasons to assume that the pore aspect ratio ε should be anything but equal to one.

[21] 2. In unconsolidated, monodisperse sphere packs, z has been determined to be very close to six [e.g., Doyen, 1988, and references therein; Peford *et al.*, 2001].

[22] 3. We are not aware of a detailed study of pore length in unconsolidated, monodisperse sphere packs. However, for this ideal material, we expect the pore length to have a relatively narrow distribution and the average pore length l to be comparable in magnitude to the grain radius R . A more precise value can be obtained by examining the pore structure of FCC sphere packing. The conductive pores connect the octahedral and tetrahedral nodal holes. Their length is approximately equal to $1.2 R$. In absence of more specific information, we simply assumed $l = 1.2 R$ for both the Glover glass beads and Biella sands.

[23] 4. BLM assigned a conservatively low value, $\sigma_r \approx 0.45$, for Fontainebleau sandstone. As will be shown in section 4.3, this value is not unreasonable for the high porosity samples but higher values may be more appropriate for low porosity Fontainebleau sandstone varieties. We surmise that unconsolidated granular materials should be quite similar to highly porous, clean sandstones, so $\sigma_r = 0.45$ seems an adequate choice. Furthermore, we note that this value ($\sigma_r = 0.45$) is consistent with the widths of the pore throat diameter distributions graphically reported by Glover and Déry [2010, Figure 6]. Finally, we point out that σ_r has a rather weak effect on the modeled values of k and F (at least in the range of σ_r considered here). For example, increasing σ_r from 0.4 to 0.5 in the kz - and

Fz -equations produces a decrease of k by a factor of 1.3 and an increase of F by a factor of 1.2, while the kF -equation is nearly unaffected.

[24] 5. As mentioned earlier, the hydraulic radius is defined as $r_H = 2V_p/A_p$. We can calculate approximate values of V_p and A_p , assuming that the grains are all identical, non-intersecting spheres with radius R . Let us consider n spheres having a total volume $V_s = n(4/3)\pi R^3$ and a total surface area $A_p = n4\pi R^2$. Since $\phi = V_p/(V_s + V_p)$, we obtain $r_H = 2R\phi/(3(1-\phi))$. Of course, the assumption of perfectly spherical grains cannot be expected to be accurate. Clearly, sand grains and even glass beads are not spherical. Given that R is defined as the radius of a sphere of equal volume to that of the actual grain, the expression mentioned above under-estimates the pore surface area A_p by a factor $f_s > 1$ and a more precise approximation of r_H is given by

$$r_H = \frac{2R\phi}{3f_s(1-\phi)}. \quad (14)$$

We emphasize that f_s is not a model parameter but merely a correcting factor intended to take care of the systematic error caused by assuming perfectly spherical grains. Obviously, there would be no need for it if direct measurements of r_H were available. f_s should evidently be very close to 1 for the Glover glass beads. It should also be insensitive to grain size. Indeed, examination of the Glover data set shows that k varied almost exactly as R^2 , whereas F and ϕ were nearly constant, relationships that can actually be derived from our model, the linear relation of l to R posited in parameter 3 and equation (14) with a R -independent f_s . For natural sand grains, on the other hand, f_s should be significantly greater than one and increase with decreasing R , since the sphericity of natural sand grains was observed to decrease with decreasing grain size [e.g., *Rogers and Head*, 1961; *Friedman*, 1962]. As a matter of fact, the Biella 1 data set did yield $k \propto R^{1.9}$, $F \propto R^{0.1}$ and $\phi \propto R^{-0.1}$, relationships consistent with the R -dependence of f_s described above. In order to estimate a plausible range of variation for f_s , we examined two-dimensional micrographs of sand grains from *Beard and Weyl* [1973]. Based on the description of the Biella sands, we ignored highly angular and/or elongated grains. Because of the very poor resolution of the printed micrographs, we only considered large grains. We used standard stereology techniques to measure the area A and perimeter P of two-dimensional grain sections. We estimated an equivalent grain radius R from A and found that P was greater than $2\pi R$ by a factor of around 1.1–1.2 for fairly equi-dimensional rounded grains, and up to 1.4 for relatively angular and elongated grains (i.e., with an aspect ratio of about 0.6). The surface area of the (three-dimensional) grains must then be greater than $4\pi R^2$ by a factor between 1.2 and 2, hence defining the expected range of variation of f_s .

[25] To determine the input values of r_H , we compared the results of two hypotheses: (1) we assumed a perfectly spherical shape of the grains (i.e., $f_s = 1$), and, (2) we allowed $f_s > 1$ to vary and estimated its value by optimization. Applying hypothesis 2 to the Glover data set, we found that the optimized f_s was constant and equal to 1.15 ± 0.1 , a value sufficiently close to one to be considered reasonable in the case of glass beads. For the Biella 1 sands, the estimated f_s values tended to increase with decreasing R , although they displayed large relative fluctuations (± 0.3)

about the general trend. We ascertained that the trend was satisfactorily approximated by $f_s = 2.0 R^{-0.06}$ (with R in μm). Given the values of R used, f_s varied from 1.2–1.5 as expected for rounded sand grains. Finally, f_s values of 1.8 and 1.9 were needed for the Biella 2 sands, consistent with their lower grain sphericity. Assumption 2 improved the fit for all three kz -, Fz -, and kF -equations. The gain in fit quality can be visually assessed in each case in Figures 2a–2c. The average numerical values of ξ_{kz} , ξ_{Fz} , and ξ_{kF} are given in Table 2, showing that the best fit is obtained for the Fz - and the worst for the Fk -equation.

4.2. Mixed, Unconsolidated Granular Media

[26] *Biella and Tabacco* [1981] and *Biella et al.* [1983] also studied binary mixtures of some of the monodisperse sands discussed above. Let us denote R_1 and R_2 the grain sizes of a binary mixture ($R_1 < R_2$ by convention), and m_1 and m_2 the corresponding weight-fractions. It is well known that the porosity of a binary sand mixture describes a V-shaped curve as illustrated in Figure 3, with the minimum corresponding to a weight-fraction of fine sand around 30% [e.g., *Biella et al.*, 1983, and references therein]. Note that the prepared mixtures were all located on the right-hand branch of the V (Figure 3). Six groups of mixtures having the same grain sizes but different weight fractions were fabricated by Biella and co-authors. Inspection of the Biella data shows that, within each group, ϕ and $1/F$ linearly increased with increasing m_1 , while k only displayed a moderate and rather irregular rise. On the other hand, the average permeability of each group strongly increased with R_1 while ϕ and F did not significantly depend on grain size. We set the input parameters as follows:

[27] 1. In the case of a binary sand mixture, equation (14) becomes

$$r_H = \frac{2\phi}{3(1-\phi)\left(\frac{m_1 f_1}{R_1} + \frac{m_2 f_2}{R_2}\right)}, \quad (15)$$

where f_1 and f_2 are the sphericity correction factors previously determined for the corresponding monodisperse sands (see section 4.1). Within each mixture group, we obtained values of r_H modestly decreasing with increasing fine sand weight-fraction m_1 , somewhat contradictory with the increase of k mentioned earlier.

[28] 2. As illustrated in Figure 3, l varies from $l \approx l_2 = 1.2 R_2$ when $m_1 = 0$ to $l \approx l_1 = 1.2 R_1$ when $m_1 = 1$, probably following some kind of S-shaped curve. In absence of any information, we simply assumed a step-function (in other words, $l = 1.2 R_1$ in all the cases considered).

[29] 3. As before, we set the pore aspect ratio ε equal to one.

[30] 4. It is likely that σ_r varies with the fraction of fine sand. Obviously, σ_r should be taken equal to 0.45 at the end-points (i.e., $m_1 = 0$ and $m_1 = 1$) but it is not intuitively clear whether it should increase (as illustrated in Figure 3) or decrease for m_1 approaching 30%. In any event, excessively large variations of σ_r should be rejected.

[31] 5. We know that $z \approx 6$ at the end-points. In between, the coordination number can only decrease (or stay constant) and it seems logical that it would reach a minimum at the same position as porosity does. Clearly, this minimum must be significantly higher than the percolation threshold (i.e., $z_c = 1.5$), but the precise value is unknown.

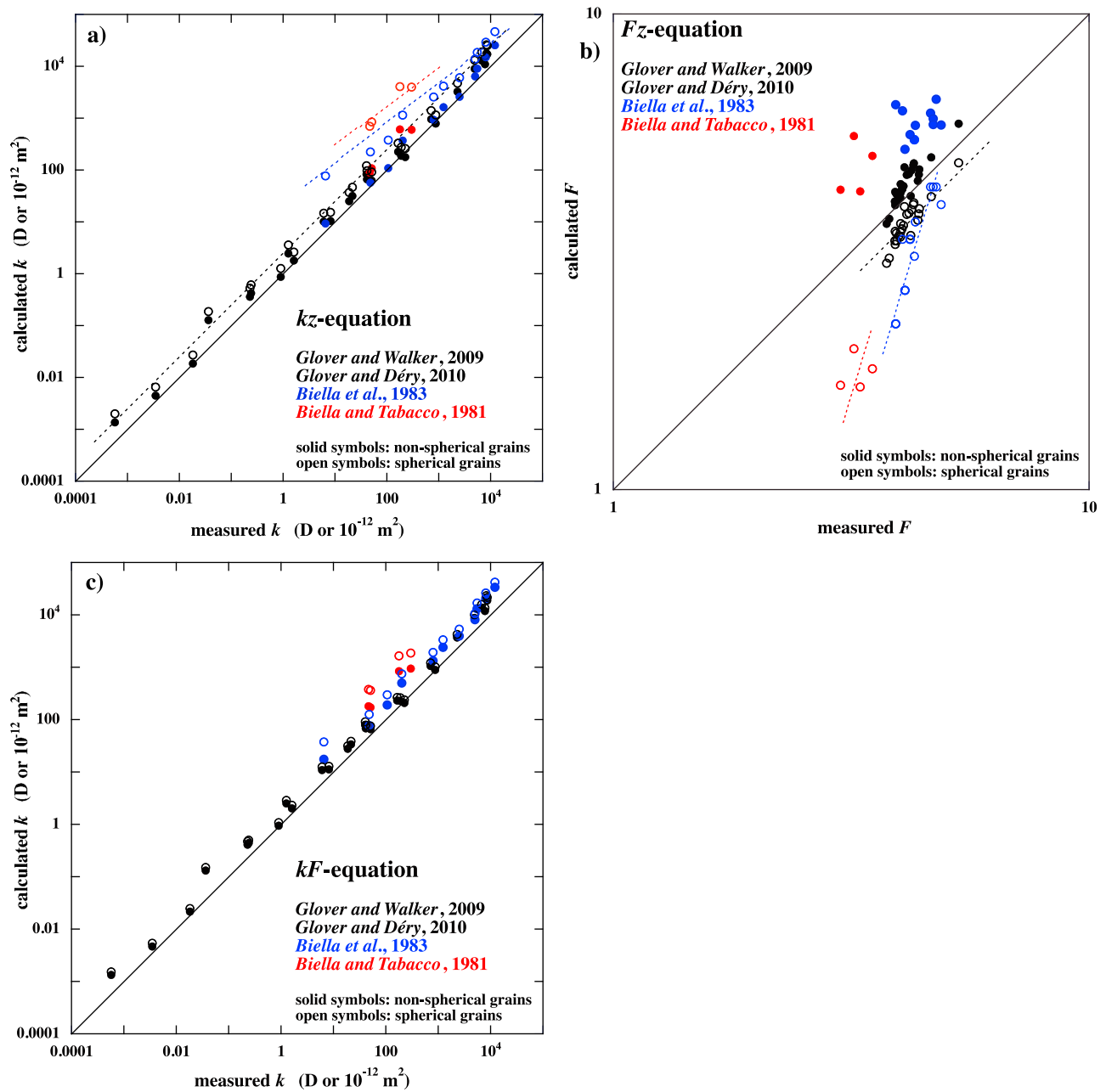


Figure 2. Comparison of calculated and measured permeability k and inverse formation factor $1/F$ for the monodisperse Glover glass beads, and the Biella 1 and Biella 2 sands (in black, blue, and red, respectively). The calculated values were obtained using (a) the kz -equation, (b) the Fz -equation, and (c) the kF -equation. The open circles correspond to assumption 1, i.e., $f_s = 1$, whereas the solid dots represent results obtained with assumption 2, i.e., $f_s > 1$, as described in the text. In the case of assumption 1, the colored dotted lines highlight the relationship between the misfit factor and R (constant misfit for Glover and increasing misfit with decreasing R for Biella 1).

Table 2. Average Fit Factors for Monodisperse Glass Beads and Sands^a

	ξ_{kz}		ξ_{Fz}		ξ_{kF}	
	Assumption 1	Assumption 2	Assumption 1	Assumption 2	Assumption 1	Assumption 2
Glover	2.3 ± 0.8	1.6 ± 0.5	1.1 ± 0.1	1.1 ± 0.04	1.9 ± 0.6	1.7 ± 0.6
Biella 1	3.7 ± 0.9	1.5 ± 0.4	1.3 ± 0.2	1.3 ± 0.10	2.9 ± 0.6	2.1 ± 0.5
Biella 2	17.0 ± 4.0	2.4 ± 0.7	1.8 ± 0.2	1.5 ± 0.20	7.8 ± 1.4	3.8 ± 0.7

^aAssumption 1, $f_s = 1$; assumption 2, $f_s > 1$. Namely, f_s does not depend on grain size for the Glover data set and is given by $f_s = 2.0 R^{-0.06}$ for Biella 1, whereas Biella 2 requires values on the order of 1.8 or 1.9; see text for details.

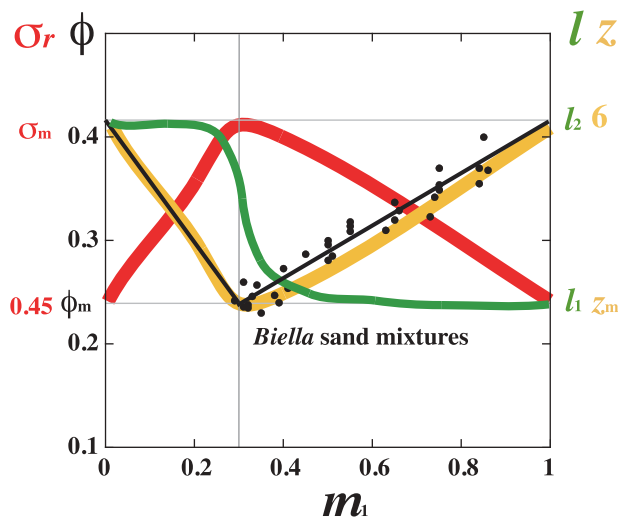


Figure 3. Porosity of the Biella binary sand mixtures plotted versus fine sand weight-fraction m_1 (black dots; the black line highlights the linear best fit relation, $\phi \approx 0.16 + 0.25 m_1$). The expected variations of pore length l , coordination number z , and pore size heterogeneity σ_r , are indicated by green, yellow, and red lines, respectively.

[32] As in section 4.1, we compared different assumptions: (1) we assumed that the mixtures behaved exactly like monodisperse sands and assigned the constant input values $z = 6$ and $\sigma_r = 0.45$, (2) we allowed z to vary while keeping σ_r equal to 0.45, and (3) we conversely allowed σ_r to vary while keeping z equal to 6. We found that the optimized values of z and σ_r could be adequately approximated by $z = 1.754 + 7.889 m_1 - 3.620 m_1^2$ and $\sigma_r = 1.110 - 1.210 m_1 + 0.561 m_1^2$ for (2) and (3), respectively. These functions give quite credible values of z (i.e., 6–3.8) and σ_r (i.e., 0.46–0.80), well within the plausible ranges.

[33] Assumptions 2 and 3 produced a major improvement in fit quality for the kz -equation, which more than compensated the small quality decline observed for the Fz -equation (see Figures 4a–4c and Table 3). Assumption 3 also ameliorated the fit for the kF -equation (in this case assumptions 1 and 2 are undistinguishable). Notice that, although assumption 1 yielded the best fit for the Fz -equation, it produced a somewhat regular increase of the individual misfit factors with m_1 (see Figure 4b). This trend suggests that the microstructure of the binary sand mixtures evolved with the fine sand weight-fraction m_1 in a way that was not accounted for by assumption 1. Assumptions 2 and 3 both removed this trend. In fact, the results of assumptions 2 and 3 were very similar not only overall but also for each individual sample (the similarity was such that we found it redundant to plot the results of assumption 3 in Figures 4a and 4b). It is therefore likely that sand mixing produced changes in either z or σ_r (or both), although we cannot determine which parameter was most important without additional information.

4.3. Fontainebleau Sandstone

[34] There is one rock, Fontainebleau sandstone, for which z and most of the other quantities needed here are available in the literature. Fontainebleau sandstone was considered in many past studies because its porosity varies over a very wide

range (i.e., 3–30%) while other characteristics such as mineralogical composition ($\sim 100\%$ quartz) and grain size remain nearly constant [e.g., Bourbié and Zinszner, 1985]. As a consequence, the physical properties of Fontainebleau sandstone display very distinctive trends when plotted against porosity [e.g., Bourbié and Zinszner, 1985]. For example, the k and $1/F$ data of Doyen [1988] and Fredrich et al. [1993] plotted in Figure 5 clearly reveal well-defined trends, even though considerable fluctuations occurred for individual samples. BLM used these trends to merge the data sets of Doyen [1988], Fredrich et al. [1993], and Lindquist et al. [2000] into a single data set containing directly measured or inferred quantities (details on the merging methods can be found in the work of Bernabé et al. [2010]). In the merged data set, the values of k and F are the results of actual measurements, while the microstructure parameters r_H , l and z are partly measured and partly inferred. It is important to remark that the natural variability of Fontainebleau sandstone, in addition to the uncertainty of the merging methods, substantially limits the modeling precision that can be expected. The BLM Fontainebleau data set contains two different estimates of z , one based on two-dimensional microstructure analysis [Doyen, 1988] and the other obtained from the medial axis analysis of three-dimensional images of the pore space [Lindquist et al., 2000]. BLM tested both versions and found that Lindquist et al.'s coordination number appeared to be considerably underestimated (probably because the medial axis method introduces a strong bias toward the low value of 3 whereas Doyen's gave very good results (probably because Doyen's z was calibrated to be equal to 6 in the most porous samples)). Here, we only used Doyen's coordination number.

[35] Thus, two unconstrained parameters remain, namely σ_r and ε . We are not aware of any study of the statistics of pore scale values of the hydraulic radius, from which σ_r could be inferred, but the statistics of a number of other microstructure attributes, such as throat and nodal pore size, were reported by Doyen [1988], Fredrich et al. [1993], and Lindquist et al. [2000]. The corresponding normalized standard deviations varied from about 0.4 to as high as 1.2, depending on the attribute considered and the porosity of the sample (in general, normalized standard deviations increased with decreasing porosity). BLM selected a value near the lower limit, $\sigma_r = 0.45$, and found that, in conjunction with $\varepsilon = 1$ (i.e., pores with equi-dimensional cross-sections), this input value produced a satisfactory fit for the kz -equation ($\xi_{kz} = 2.0 \pm 0.9$; see Figure 6a). Applying the same values, $\sigma_r = 0.45$ and $\varepsilon = 1$, to the Fz - and kF -equations, we discovered, however, that the good fit observed by BLM was not a robust result. For each data point, the individual misfit factors ξ_{Fz} and ξ_{kF} were relatively small for the high porosity samples but grew to unacceptable levels at low porosities (e.g., nearly two orders of magnitude for k when porosity reaches 5%; see Figures 6b and 6c). One way to reconcile the k and F data is to take into account the pore shape variations observed in Fontainebleau sandstone. Micrographs of different varieties of Fontainebleau sandstone by Bourbié and Zinszner [1985] show that porosity reduction was associated with an evolution of the pore cross-section from approximately equi-dimensional to thin and elongated. In particular, thin inter-granular crack-like pores are prevailing in the pore casts of very low porosity samples [see Bourbié

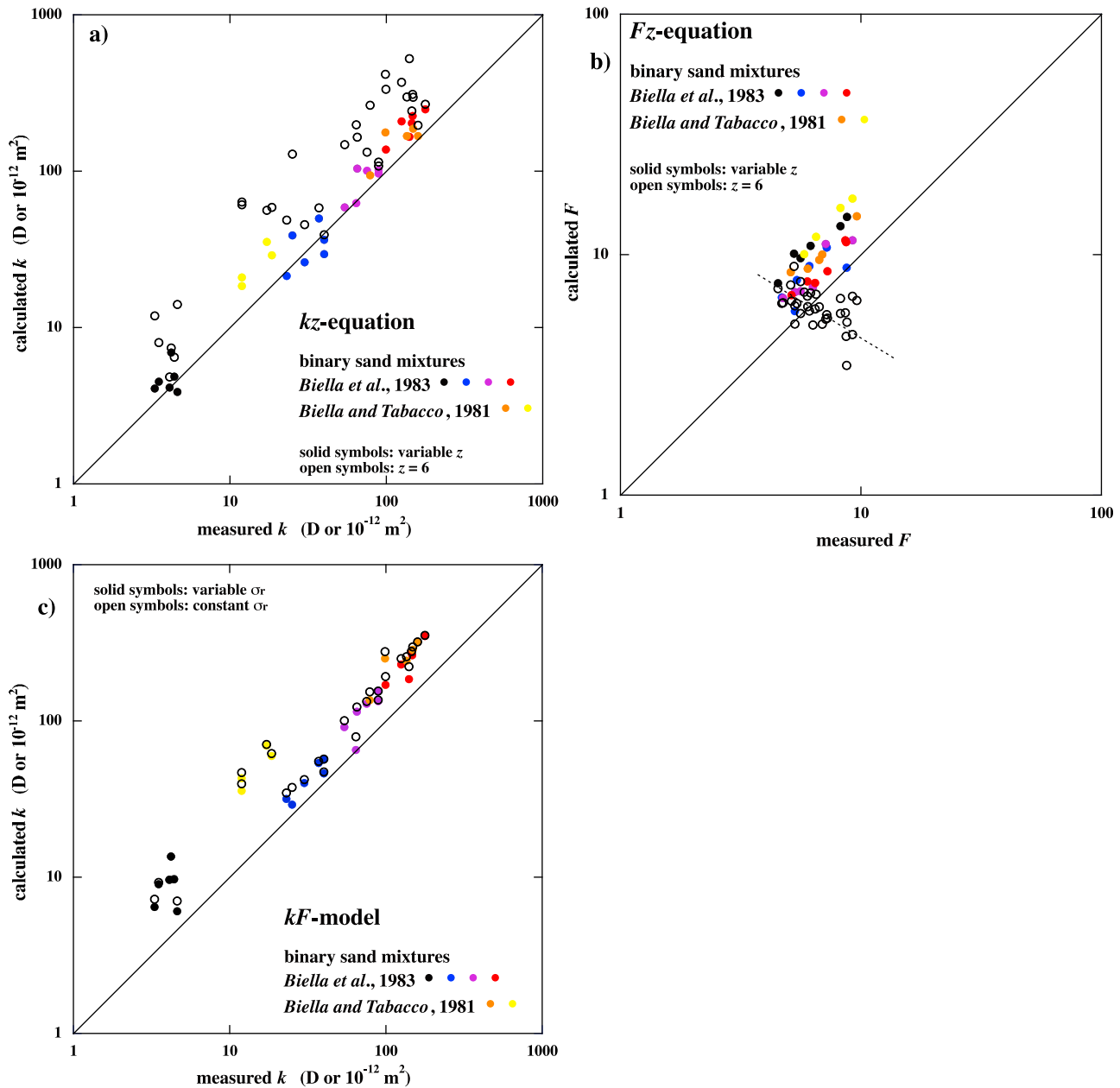


Figure 4. Comparison of calculated and measured k and $1/F$ for the Biella binary sand mixtures (the various groups of mixtures are represented with different colors). The calculated values were obtained using (a) the kz -equation, (b) the Fz -equation, and (c) the kF -equation. For Figures 4a and 4b, the open circles correspond to assumption 1, i.e., constant $z = 6$ and $\sigma_r = 0.45$, and the solid dots to assumption 2, i.e., variable z (see text). The dotted line in Figure 4b highlights the dependence of the misfit factor on F (and therefore m_1), when assumption 1 is used (see text). For Figure 4c, open circles and solid dots respectively represent the results obtained using assumption 1 and assumption 3, i.e., variable σ_r (see text). In order to avoid impairing visibility the open symbols are all plotted in black.

Table 3. Average Fit Factors for Binary Mixtures of Sands^a

ξ_{kz}			ξ_{Fz}			ξ_{kF}		
Assumption 1	Assumption 2	Assumption 3	Assumption 1	Assumption 2	Assumption 3	Assumption 1	Assumption 2	Assumption 3
2.3 ± 1.1	1.2 ± 0.2	1.2 ± 0.2	1.4 ± 0.4	1.6 ± 0.3	1.5 ± 0.2	2.1 ± 0.7	2.1 ± 0.7	1.7 ± 0.3

^aAssumption 1, $z = 6$ and $\sigma_r = 0.45$; assumption 2, $z = 1.754 + 7.889 m_1 - 3.620 m_1^2$ and $\sigma_r = 0.45$; assumption 3, $\sigma_r = 1.110 - 1.210 m_1 + 0.561 m_1^2$ and $z = 6$. See text for details.

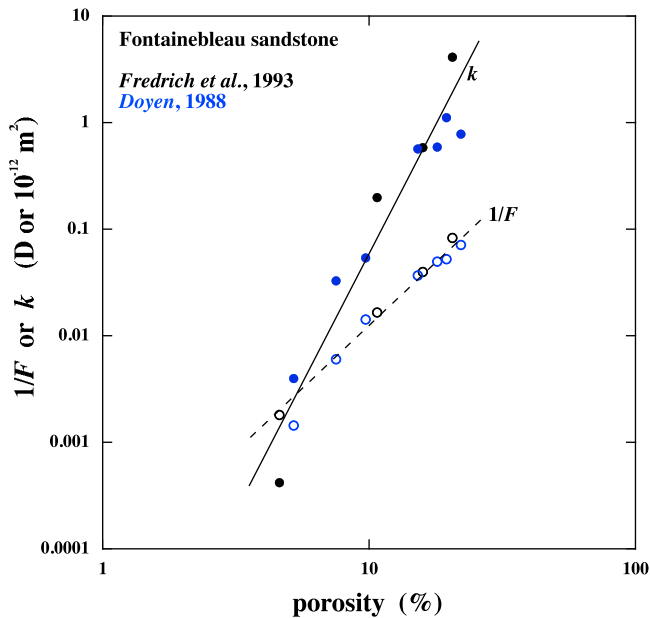


Figure 5. Illustration of the merged Fontainebleau sandstone data set. Permeability (solid dots) and inverse formation factor (open circles) are plotted versus porosity. The data originate from *Fredrich et al.* [1993] (black) and *Doyen* [1988] (blue). The general, well-defined trends are highlighted by the solid and dotted lines.

and *Zinszner*, 1985, Figure 20]. The predominance of flattened pores in low porosity Fontainebleau sandstone is also supported by an observed large pressure-sensitivity of k and F [e.g., *Fredrich et al.*, 1993; *Gomez et al.*, 2010]. Adjusting the pore aspect ratio ε alone is not sufficient, however, since it would destroy the good fit observed by BLM for the kz -equation. The only solution allowed by the model is to couple a decrease of ε with a simultaneous increase of σ_r , a plausible option since an increase of pore scale heterogeneity was generally observed to accompany porosity loss in Fontainebleau sandstone [see, e.g., *Bourbié and Zinszner*, 1985, Figure 2].

[36] We therefore tried to optimize σ_r and ε jointly. We considered 4 groups of 2 or 3 samples of similar porosities (i.e., 22–19.5%, 18–15%, 11–7.5%, and 5%). For each group, we explored the variations of the global misfit factor (i.e., the geometric average of ξ_{kz} , ξ_{Fz} , and ξ_{kF}) in the entire $[\sigma_r, \varepsilon]$ plane. Because of the variability/uncertainty issue mentioned earlier, we did not expect the location in $[\sigma_r, \varepsilon]$ space of the minimum of the misfit factor to be truly representative. Instead, we plotted the iso- ξ contour lines corresponding to misfit factors of 1.8, 1.5, 1.7, and 2.4 for the 20%, 16%, 9%, and 5% groups, respectively (see Figure 7). These lines delimit zones in the $[\sigma_r, \varepsilon]$ plane where a reasonable fit can be found. They were constructed to be neither too large (i.e., insufficiently discriminating) nor too small (i.e., too sensitive to experimental errors and uncertainties). For each sample, we then selected values of σ_r and ε falling within the appropriate fitting zones (see Figure 7) and consistent with the microstructure evolution of Fontai-

nebleau sandstone described in the preceding paragraph. For the sample with the highest porosity, $\sigma_r = 0.45$ is a reasonable value, as already discussed, while $\varepsilon = 0.4$ is compatible with the moderately low pressure dependence of k and F observed in highly porous Fontainebleau sandstone (elliptical, infinitely thick-walled pipes have negligible pressure sensitivities for aspect ratios from about 0.6–1, but become too compressible for $\varepsilon < 0.1$) [e.g., *Bernabé et al.*, 1982]. With decreasing porosity, we assumed that pore size heterogeneity regularly increased while the pore aspect ratio simultaneously decreased (toward the low porosity end-values of $\sigma_r = 0.85$ and $\varepsilon = 0.02$). Using the input parameters shown in Figure 7 preserved the fit obtained by BLM for the kz -equation ($\xi_{kz} = 1.8 \pm 0.7$; see Figure 6a) and, furthermore, greatly improved it for the Fz - and kF -equations ($\xi_{Fz} = 1.3 \pm 0.4$ and $\xi_{kF} = 2.1 \pm 1.1$; see Figures 6b and 6c), although discrepancies of up to half of an order of magnitude still occurred. Most importantly, the fit quality was roughly the same for all samples, regardless of their permeability.

4.4. Fused Glass Beads and Various Sandstones

[37] Although z is essentially unknown for rocks other than Fontainebleau sandstone, the kF -equation can still be tested in rocks for which enough data on k , F , and the most important microstructure attributes are available. For example, *Blair et al.* [1996] measured ϕ , k , F , the mean grain radius R (yielding $l \approx 1.2 R$ as for unconsolidated granular media), and the specific surface area of the pores, from which r_H can be calculated, in samples of fused glass beads with porosity varying from 17 to 39%, and in natural sandstones with ϕ between 11 and 22% (namely, Berea, Frontier, Tensleep, Navajo, and Flathead sandstones). *Zhan et al.* [2010] made similar measurements on a sample of Berea sandstone with porosity of 23.6%. Furthermore, they acquired three-dimensional images of the sample pore space using X-ray microtomography. These images were analyzed to determine the local values of the microstructure attributes and were also used to run numerical simulations of hydraulic flow and electrical conduction (assuming zero surface conduction), allowing estimation of the corresponding values of k and F . *Zhan et al.*'s [2010] simulations yielded slight overestimates of both k and F with respect to the experimental measurements. They did not report values of mean pore length (or of mean grain radius), and we decided to use $R = 65 \mu\text{m}$, a value corresponding to the middle of the range covered by the Berea sandstone samples used by *Blair et al.* [1996]. As in the Fontainebleau sandstone case, we lack specific, precise information on σ_r and ε . Therefore, we systematically explored the $[\sigma_r, \varepsilon]$ plane as explained in the preceding section. The contour lines corresponding to $\xi_{kF} = 1.24$ and 1.4 determined for various groups of samples (Figure 8) suggest that the natural sandstones and the fused glass beads with $\phi > 20\%$ have relatively similar behaviors, while the fused glass beads sample with $\phi = 17\%$ comes out as an anomaly. The natural sandstones data are consistent with σ_r around 0.6, a value in the middle of the range previously found for Fontainebleau sandstone, and tend to favor high aspect ratios. The data for the high-porosity fused glass beads samples are not incompatible with these values, although higher σ_r 's and

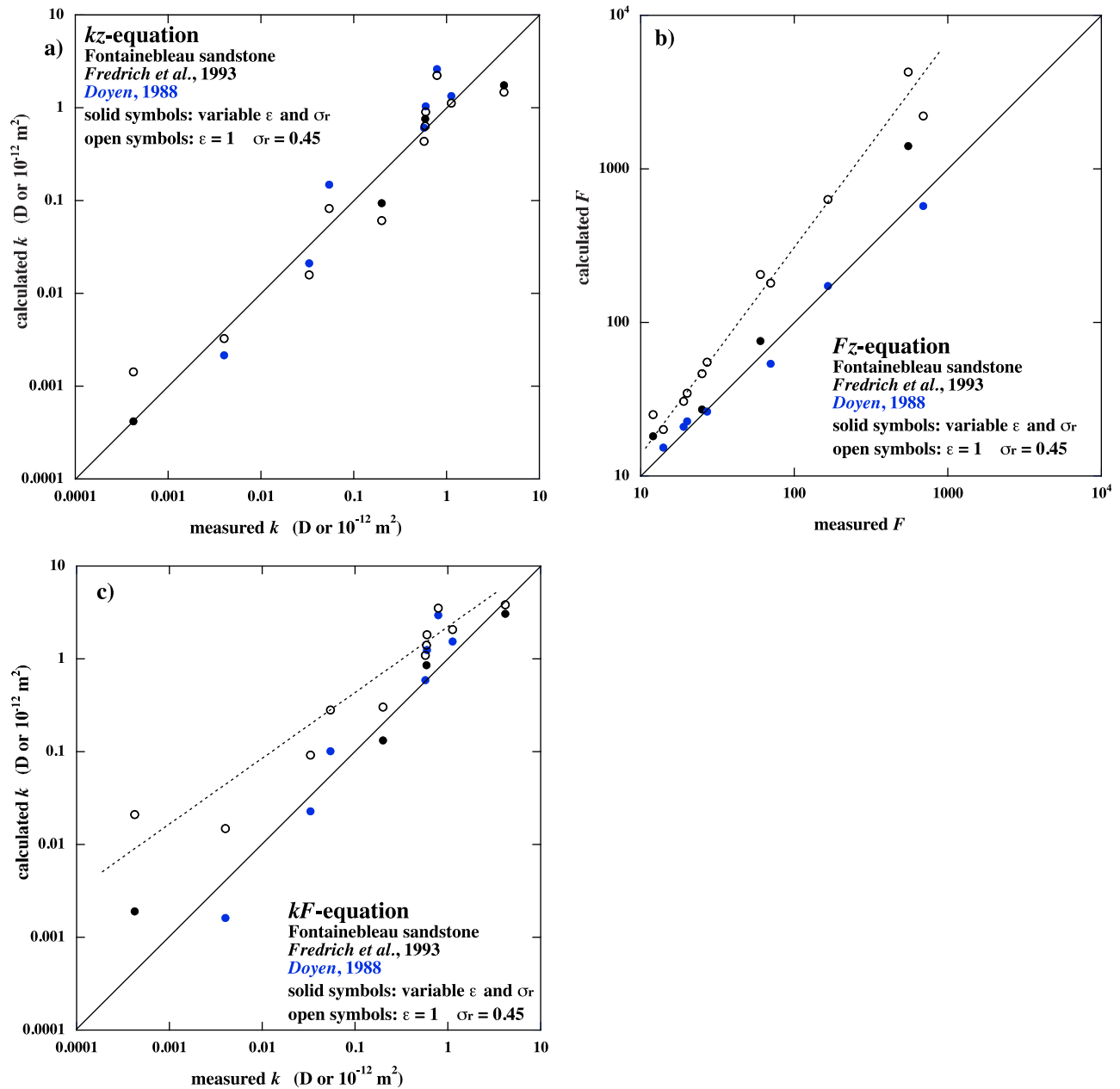


Figure 6. Comparison of calculated and measured k and $1/F$ for Fontainebleau sandstone (black symbols, Fredrich *et al.* [1993]; blue symbols, Doyen [1988]). The calculated values were obtained using (a) the kz -equation, (b) the Fz -equation, and (c) the kF -equation. The open circles correspond to the assumption of constant $\varepsilon = 1$ and $\sigma_r = 0.45$ (the large increase of the misfit factors with decreasing permeability is highlighted by the dotted lines) and the solid dots to coupled variations of ε and σ_r as described in the text.

lower ε 's would yield a slightly better fit. The data corresponding to the fused glass beads sample with $\phi = 17\%$ appears to be rather insensitive to σ_r , but needs ε near 0.1 to achieve the same level of fit as the other samples. The microstructure image of Blair *et al.* [1996, Figure 3b] shows pores with aspect ratios as low as 0.1, apparently supporting this last observation. But it can be objected that, in a two-dimensional micrograph, cross and longitudinal sections of pores cannot be distinguished, and, the measured pore

aspect ratio ε is therefore underestimated. Alternatively, the anomalous behavior of this sample may have simply been caused by experimental errors. In order to simplify the analysis, we finally assumed a single pair of values, $\sigma_r = 0.6$ and $\varepsilon = 0.7$, for all the samples in the Blair and Zhan data sets (see Figure 8). We found that the kF -equation produced generally good results over 4 orders of magnitude of measured permeability ($\xi_{kF} = 1.3 \pm 0.4$; see Figure 9), giving

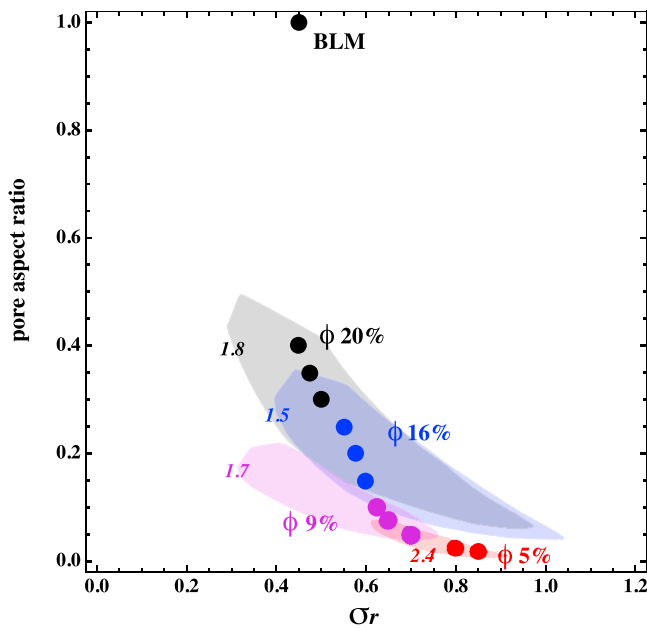


Figure 7. Regions in $[\sigma_r, \varepsilon]$ parameter space where a reasonably good fit with the Fontainebleau sandstone data can be found. These regions are limited by contour lines corresponding to misfit factors equal to 1.8 (gray), 1.5 (blue), 1.7 (purple), and 2.4 (red) for the 20%, 16%, 9%, and 5% porosity groups, respectively. The input values of σ_r and ε corresponding to the solid dots in Figure 6 are indicated by solid dots in colors matching that of the group. For comparison, the BLM input values, $\sigma_r = 0.45$ and $\varepsilon = 1$, are also represented by the black dot labeled BLM.

credence to the idea that F can effectively be used to make up for a lack of information on z .

5. Discussion

[38] How successful is the model? There are a number of positive arguments: We obtained satisfactory results, (1) over about seven orders of magnitude of permeability, (2) for a broad variety of granular materials and rocks (of course, other important types of rocks, e.g., carbonates, still need to be tested), and (3) while always maintaining the poorly constrained input parameters within tightly defined, plausible bounds. Given the fact that poorly constrained parameters were unavoidable, we paid particular attention to this last issue. We carefully proceeded in two stages: (1) starting with the simplest assumptions and, therefore, selecting relatively crude estimates of the unknown input parameters, then (2) refining the input parameters based on additional, independent information. For example, in the case of well-sorted granular media, we first assumed a perfect spherical shape of the grains, and then introduced a correction factor for the sphericity imperfections expected in glass beads and natural sand grains. In support for the model, the more credible and realistic hypotheses used in the second stage improved the fit quality in all cases considered.

[39] Considering the kF -equation in isolation, the satisfactory fit generally found in all materials, indicates that F can effectively make up for a lack of quantitative informa-

tion on z . Furthermore, the kF -equation performed better than its counterpart in the equivalent channel model (EMC) of Paterson [1983] and Walsh and Brace [1984] (i.e., $k = r_{th}^2/bF$, where b is a geometric factor equal to 8 for cylindrical pipes and 12 for cracks). Our model yielded a significant gain in fit quality with respect to EMC for the Blair and Zhan rocks and fused glass beads ($\xi_{kF} = 1.3 \pm 0.3$ compared to $\xi_{EMC} = 2.0 \pm 0.8$) and the binary sand mixtures ($\xi_{kF} = 1.7 \pm 0.3$ compared to $\xi_{EMC} = 2.6 \pm 0.9$), while both models worked equally well for the well-sorted glass beads and sands. The case of Fontainebleau sandstone was particularly illuminating. We obtained an approximately constant fit corresponding to $\xi_{kF} = 2.8 \pm 2.6$ in the entire porosity range, whereas EMC overestimated permeability in all samples by factors that gradually increased with decreasing ϕ , up to nearly 100 for the sample with the lowest porosity (the average misfit factor ξ_{EMC} was much larger than ξ_{kF} , i.e., $\xi_{EMC} = 16 \pm 30$ and 11 ± 20 for $b = 8$ and 12, respectively).

[40] Another important characteristic of the model is that its physical basis requires all three constituent equations to be satisfied simultaneously. Owing to this powerful principle, the model can be applied even in cases where some input parameters are essentially unknown. For example, in the case of Fontainebleau sandstone, we were able to fit the kz -, Fz -, and kF -equations all together, by replacing the unrealistically simple assumptions used by BLM (i.e., equidimensional pores and low pore size heterogeneity for all porosities) by a set of coupled values of σ_r and ε , qualitatively consistent with the evolution of the microstructure of Fontainebleau sandstone observed in previous studies

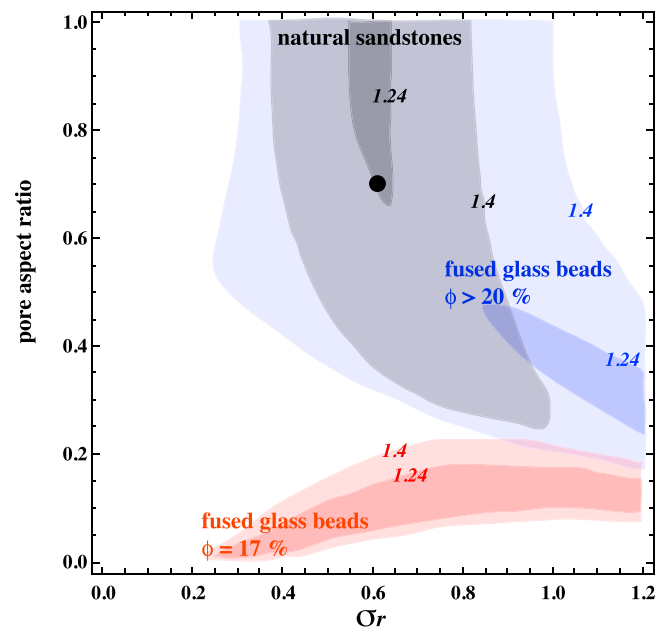


Figure 8. Regions in $[\sigma_r, \varepsilon]$ parameter space where a reasonably good fit with the Blair and Zhan data can be found. These regions are limited by contour lines corresponding to misfit factors equal to 1.4 (lighter colors) and 1.24 (darker colors). The natural sandstones are represented in gray, the fused glass beads with $\phi > 20\%$ in blue, and the anomalous fused glass beads sample with $\phi = 17\%$ in red. Our choice of input parameters is indicated by the black solid dot.

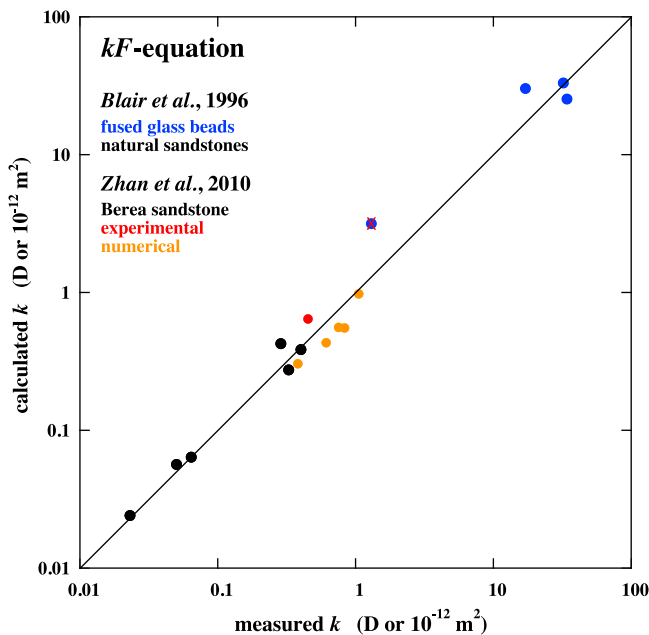


Figure 9. Comparison of calculated and measured k for the Blair and Zhan data sets (natural sandstones from Blair *et al.* [1996], black solid dots; fused glass beads from Blair *et al.* [1996], blue solid dots, anomalous sample highlighted with a red X; Berea sandstone from Zhan *et al.* [2010], experimental data, red solid dot; numerical simulations, orange solid dots). The calculated values were obtained using the kF -equation with the input values of ε and σ_r shown in Figure 8.

[Bourbié and Zinszner, 1985; Doyen, 1988; Fredrich *et al.*, 1993; Lindquist *et al.*, 2000].

[41] As pointed out in section 3, porosity does not appear explicitly in our model. Nevertheless, it is worthwhile to check if the model is consistent with Archie's law, $F = \phi^{-m}$, where m is called the cementation exponent and ranges between one and four for most soils and rocks. Incorporating Archie's law into the Fz -equation yields

$$m = \frac{\log C_F + 2 \log \left(\frac{r_H}{l} \right) + \gamma \log(z - z_c)}{\log \phi}. \quad (16)$$

Examination of equation (16) shows that the predicted cementation exponent tends to increase with decreasing connectivity and/or increasing heterogeneity (C_F decreases with increasing σ_r). The effect of ϕ and r_H/l cannot be assessed easily because they are not independent quantities. Applying equation (16) to Fontainebleau sandstone, we found that the experimental and predicted values of m were very similar, both increasing from ~ 1.6 to ~ 2.3 with decreasing ϕ . Of course, this good agreement merely reflects the fact, already discussed, that our model adequately predicted F .

[42] In the case of the unconsolidated granular media of sections 4.1 and 4.2, r_H/l can be expressed as a function of ϕ :

$$\frac{r_H}{l} = \frac{\phi}{1.8(1 - \phi) \left(m_1 f_1 + m_2 f_2 \frac{R_2}{R_1} \right)}. \quad (17)$$

Equation (17) reduces to $\phi/1.8f_s(1-\phi)$ for monodisperse sands. In good agreement with the prediction of Sen *et al.* [1981] (i.e., $m = 1.5$), the observed cementation exponents were 1.51 ± 0.03 , 1.59 ± 0.06 , and 1.60 ± 0.09 for the Glover glass beads, the Biella 1, and Biella 2 sands, respectively (note that m showed a slight increase with decreasing R for the Biella 1 sands, consistent with the trends mentioned in previous sections). Our model underestimated m when $f_s = 1$ was assumed (1.46 ± 0.06 for Glover, 1.43 ± 0.15 for Biella 1, and 0.89 ± 0.09 for Biella 2) but yielded significant overestimates when $f_s > 1$ was used (1.76 ± 0.05 for Glover, 2.12 ± 0.17 for Biella 1, and 2.56 ± 0.10 for Biella 2). This suggests that our attempt to model k and F simultaneously led to an overcorrection of grain sphericity (i.e., a too large f_s). One way to reconcile the k and F data is to reconsider our assumption that pores can be modeled as cylindrical pipes. In reality, pores in granular media have relatively wide cross-sections at their extremities, where they connect to nodal pores, and become substantially narrower at mid-length (often called "throat"). For a given value of the local hydraulic radius, this shape corresponds to hydraulic and electric conductances, $g_i^{(h)}$ and $g_i^{(e)}$, lower than predicted by equations (3) and (7). Most importantly, the effect is more pronounced for $g_i^{(h)}$ than $g_i^{(e)}$, thus reducing the discrepancy described above. For example, let's consider a pore in the form of a double conical frustum with radii $r_{\text{node}} \approx 0.15l$ at the ends and $r_{\text{throat}} \approx 0.6r_{\text{node}}$ at the center. This idealized pore geometry yields a reduction of $g_i^{(h)}$ by a factor of about 0.75 and $g_i^{(e)}$ by 0.9 with respect to the $g_i^{(h)}$ and $g_i^{(e)}$ values for a cylindrical pore with an identical hydraulic radius. As a test, we incorporated the products $0.75C_k$, $0.9C_F$, and the appropriate value for C_0 in the kz -, Fz -, and kF -equations. We found that it was, indeed, much easier to fit the modified equations to the Glover and Biella data than the original ones, the misfit factors were all reduced and smaller sphericity correction factors f_s were generally required. Notice that, unlike the correction factor f_s , the ratios r_{node}/l and $r_{\text{throat}}/r_{\text{node}}$ are genuine scale-invariant quantities that may ultimately have to be included in models of k and F , especially if very accurate predictions are sought. It must be recognized, however, that such minor effects are taken into account at the price of augmenting the model degrees of freedom, thus reducing its practical usefulness.

[43] Finally, we applied equations (16) and (17) to the Biella binary sand mixtures, for which ϕ and F strongly depend on the fine sand weight-fraction m_1 (the empirical relations are $\phi \approx 0.16 + 0.25 m_1$ and $F \approx 14 - 21 m_1 + 12 m_1^2$, see Figure 3). As shown in Figure 10, the experimentally measured m slightly increased with m_1 from ~ 1.5 for $m_1 = 0.3$ to ~ 1.6 for the monodisperse fine sands. In order to analyze our model response, we plugged the empirical $\phi - m_1$ transform mentioned above into equations (16) and (17). We considered the same cases as in section 4.2, namely, (1) constant values $z = 6$ and $\sigma_r = 0.45$, (2) variable z and $\sigma_r = 0.45$, and (3) $z = 6$ and variable σ_r (note that, for simplicity sake, we used constant $f_1 = f_2 = 1.2$ in all cases). Case 1 produced an overly steep decrease of m with decreasing m_1 . On the other hand, cases 2 and 3 showed that a significant improvement was obtained by using m_1 -dependent parameters. Thus, it seems likely that other scale-invariant parameters such as r_{node}/l and

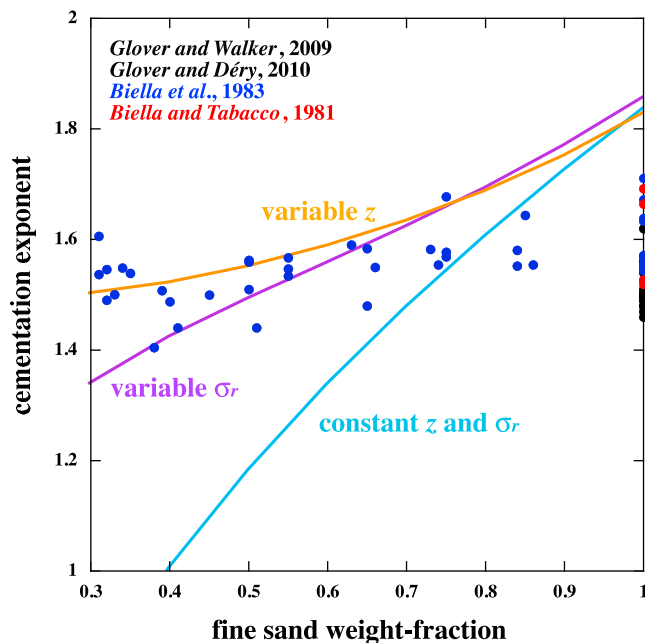


Figure 10. Cementation exponent as a function of fine sand weight-fraction for the Biella binary sand mixtures (blue solid dots). The values for the Glover monodisperse ($m_1 = 1$) glass beads (black solid dots) and the Biella sands (blue and red solid dots) are also indicated. The colored solid lines represent the model prediction corresponding to the various input models discussed in the text (i.e., constant z and σ_r , light blue; variable z , orange; variable σ_r , purple). These lines were obtained using the empirical relation, $\phi \approx 0.16 + 0.25 m_1$.

$r_{\text{throat}}/r_{\text{node}}$ may have to be added to the model to generate more accurate predictions for binary sand mixtures.

6. Conclusions

[44] 1. In three-dimensional networks, permeability and formation factor obey “universal” power laws of z - z_c in the entire domain of variation of z except very near the percolation threshold z_c . The exponents of these power laws as well as the pre-factors are strongly dependent on pore size heterogeneity.

[45] 2. A joint permeability-formation factor model was inferred from these power laws, using the hydraulic radius r_H as length scale and containing four scale-invariant parameters; namely, z the mean coordination number, σ_r the normalized standard deviation of the pore hydraulic radii distribution, the ratio r_H/l and the aspect ratio ε of the pore cross-sections. This model consists of three equations, the first two expressing the relationships of k and F with z - z_c , and the third one, obtained by elimination of z - z_c , linking k to F .

[46] 3. The model was satisfactorily tested on a variety of granular materials and rocks, for which the model parameters either were actually measured or could be reliably inferred.

[47] 4. Although it does not explicitly include porosity, the model is not inconsistent with Archie’s law. With our choice of input parameters, the cementation exponent was generally over-predicted but it seems that more accurate

values can be obtained if more realistic pore geometries are considered.

Appendix A

[48] The following empirically established formulas provide approximate expressions of the exponents and pre-factors of the kz -, Fz - and kF -equations as functions of σ_r and ε .

$$\beta = 1.2343 + 0.93462\sigma_r + 1.4755\sigma_r^2 \quad (\text{A1})$$

$$\gamma = 1.2903 + 0.045527\sigma_r + 0.82390\sigma_r^2 \quad (\text{A2})$$

$$\alpha = \frac{\beta}{\gamma} \quad (\text{A3})$$

$$C_k = \frac{[3(1 + \varepsilon) - \sqrt{3\varepsilon^2 + 10\varepsilon + 3}]^4}{8\varepsilon(1 + \varepsilon^2)} 10^{-(1.1950 + 0.82190\sigma_r + 2.0459\sigma_r^2)} \quad (\text{A4})$$

$$C_F = \frac{[3(1 + \varepsilon) - \sqrt{3\varepsilon^2 + 10\varepsilon + 3}]^2}{4\varepsilon} 10^{-(0.32894 + 0.23339\sigma_r + 1.1423\sigma_r^2)} \quad (\text{A5})$$

$$C = C_k C_F^{-\alpha} \quad (\text{A6})$$

[49] **Acknowledgments.** YB is grateful to André Revil for illuminating discussions. The comments and questions of Joerg Renner, Dan Faulkner, and an anonymous reviewer were very helpful to improve our manuscript. This work was partially funded by the U.S. Department of Energy under grant DE-FG09-97ER14760, and by the Open Fund PLN0901 of the State Key Laboratory of Oil and Gas Reservoir Geology and Exploitation (Southwest Petroleum University, Chengdu, China). This is IGP contribution 3207.

References

- Baldwin, C. A., A. J. Sederman, M. D. Mantle, P. Alexander, and L. F. Gladden (1996), Determination and characterization of the structure of a pore space from 3D volume images, *J. Colloid Interface Sci.*, *181*, 79–92, doi:10.1006/jcis.1996.0358.
- Beard, D. C., and P. K. Weyl (1973), Influence of texture on porosity and permeability of unconsolidated sand, *Am. Assoc. Pet. Geol. Bull.*, *57*, 349–369.
- Bernabé, Y. (1998), Streaming potential in heterogeneous networks, *J. Geophys. Res.*, *103*, 20,827–20,841, doi:10.1029/98JB02126.
- Bernabé, Y., W. F. Brace, and B. Evans (1982), Permeability, porosity and pore geometry of hot-pressed calcite, *Mech. Mater.*, *1*, 173–183, doi:10.1016/0167-6636(82)90010-2.
- Bernabé, Y., U. Mok, and B. Evans (2003), Permeability, -porosity relationships in rocks subjected to various evolution processes, *Pure Appl. Geophys.*, *160*, 937–960, doi:10.1007/PL00012574.
- Bernabé, Y., M. Li, and A. Mainault (2010), Permeability and pore connectivity: A new model based on network simulations, *J. Geophys. Res.*, *115*, B10203, doi:10.1029/2010JB007444.
- Bernard, M. L., M. Zamora, Y. Gérard, and G. Boudon (2007), Transport properties of pyroclastic rocks from Montagne Pelée volcano (Martinique, Lesser Antilles), *J. Geophys. Res.*, *112*, B05205, doi:10.1029/2006JB004385.
- Berryman, J. G. (1992a), Effective stress for transport properties of inhomogeneous porous rock, *J. Geophys. Res.*, *97*, 17,409–17,424, doi:10.1029/92JB01593.
- Berryman, J. G. (1992b), Exact effective-stress rules in rock mechanics, *Phys. Rev. A*, *46*(6), 3307–3311, doi:10.1103/PhysRevA.46.3307.

- Berryman, J. G. (1993), Effective-stress rules for pore-fluid transport in rocks containing two minerals, *Int. J. Mech. Min. Sci. Geomech. Abstr.*, *30*, 1165–1168, doi:10.1016/0148-9062(93)90087-T.
- Biella, G., and I. Tabacco (1981), The influence of grain size on the relations between resistivity, porosity and permeability in unconsolidated formations, *Boll. Geofis. Teor. Appl.*, *23*, 43–58.
- Biella, G., A. Lozej, and I. Tabacco (1983), Experimental study of some hydrogeophysical properties of unconsolidated porous media, *Ground Water*, *21*, 741–751, doi:10.1111/j.1745-6584.1983.tb01945.x.
- Blair, S. C., P. A. Berge, and J. G. Berryman (1996), Using two-point correlation functions to characterize microgeometry and estimate permeabilities of sandstones and porous glass, *J. Geophys. Res.*, *101*, 20,359–20,375, doi:10.1029/96JB00879.
- Bourbié, T., and B. Zinszner (1985), Hydraulic and acoustic properties as a function of porosity in Fontainebleau sandstone, *J. Geophys. Res.*, *90*, 11,524–11,532, doi:10.1029/JB090iB13p11524.
- Brace, W. F. (1980), Permeability of crystalline and argillaceous rocks, *Int. J. Mech. Min. Sci. Geomech. Abstr.*, *17*, 241–251, doi:10.1016/0148-9062(80)90807-4.
- David, C. (1993), Geometry of flow paths for fluid transport in rocks, *J. Geophys. Res.*, *98*, 12,267–12,278, doi:10.1029/93JB00522.
- Doyen, P. M. (1988), Permeability, conductivity, and pore geometry of sandstone, *J. Geophys. Res.*, *93*, 7729–7740, doi:10.1029/JB093iB07p07729.
- Fredrich, J. T. (1999), 3D imaging of porous media using laser scanning confocal microscopy with application to microscale transport processes, *Phys. Chem. Earth Part A*, *24*, 551–561, doi:10.1016/S1464-1895(99)00079-4.
- Fredrich, J. T., and W. B. Lindquist (1997), Statistical characterization of the three-dimensional microgeometry of porous media and correlation with macroscopic transport properties, *Int. J. Rock Mech. Min. Sci. Geomech. Abstr.*, *34*, 1–12.
- Fredrich, J. T., K. H. Greaves, and J. W. Martin (1993), Pore geometry and transport properties of Fontainebleau sandstone, *Int. J. Mech. Min. Sci. Geomech. Abstr.*, *30*, 691–697, doi:10.1016/0148-9062(93)90007-Z.
- Friedman, G. M. (1962), On sorting, sorting coefficients and the lognormality of the grain-size distribution of sandstones, *J. Geol.*, *70*, 737–753.
- Glover, P. W. J. (2009), What is the cementation exponent? A new interpretation, *Lead. Edge*, *28*, 82–85, doi:10.1190/1.3064150.
- Glover, P. W. J., and N. Déry (2010), Streaming potential coupling coefficient of quartz glass bead packs: Dependence on grain diameter, pore size, and pore throat radius, *Geophysics*, *75*, F225–F241, doi:10.1190/1.3509465.
- Glover, P. W. J., and E. Walker (2009), Grain-size to effective pore-size transformation derived from electrokinetic theory, *Geophysics*, *74*, E17–E29, doi:10.1190/1.3033217.
- Gomez, C. T., J. Dvorkin, and T. Vanorio (2010), Laboratory measurements of porosity, permeability, resistivity, and velocity on Fontainebleau sandstones, *Geophysics*, *75*, E191–E204, doi:10.1190/1.3493633.
- Guéguen, Y., and J. Dienes (1989), Transport properties of rocks from statistics and percolation, *Math. Geol.*, *21*, 1–13, doi:10.1007/BF00897237.
- Lindquist, W. B., and A. Venkatarangan (1999), Investigating 3D geometry of porous media from high resolution images, *Phys. Chem. Earth Part A*, *24*, 593–599, doi:10.1016/S1464-1895(99)00085-X.
- Lindquist, W. B., S. M. Lee, D. A. Coker, K. W. Jones, and P. Spanne (1996), Medial axis analysis of void structure in three-dimensional tomographic images of porous media, *J. Geophys. Res.*, *101*, 8297–8310, doi:10.1029/95JB03039.
- Lindquist, W. B., A. Venkatarangan, J. Dunsmuir, and T.-f. Wong (2000), Pore and throat size distributions measured from synchrotron X-ray tomographic images of Fontainebleau sandstones, *J. Geophys. Res.*, *105*, 21,509–21,527, doi:10.1029/2000JB900208.
- Paterson, M. S. (1983), The equivalent channel model for permeability and resistivity in fluid-saturated rocks—a reappraisal, *Mech. Mater.*, *2*, 345–352, doi:10.1016/0167-6636(83)90025-X.
- Petford, N., G. Davidson, and J. A. Miller (2001), Investigation of the petrophysical properties of a porous sandstone sample using confocal scanning laser microscopy, *Petrol. Geosci.*, *7*, 99–105, doi:10.1144/ptgeo.7.2.99.
- Revil, A. (1999), Ionic diffusivity, electrical conductivity, membrane and thermoelectric potentials in colloids and granular porous media: A unified model, *J. Colloid Interface Sci.*, *212*, 503–522, doi:10.1006/jcis.1998.6077.
- Revil, A. (2002), The hydroelectric problem of porous rock: Thermodynamic approach and introduction of a percolation threshold, *Geophys. J. Int.*, *151*, 944–949, doi:10.1046/j.1365-246X.2002.01815.x.
- Revil, A., and L. M. Cathles (1999), Permeability of shaly sands, *Water Resour. Res.*, *35*, 651–662, doi:10.1029/98WR02700.
- Revil, A., and P. W. J. Glover (1997), Theory of ionic surface electrical conduction in porous media, *Phys. Rev. B*, *55*, 1757–1773, doi:10.1103/PhysRevB.55.1757.
- Revil, A., and P. W. J. Glover (1998), Nature of surface electrical conductivity in natural sands, sandstones and clays, *Geophys. Res. Lett.*, *25*, 691–694, doi:10.1029/98GL00296.
- Rogers, J. J. W., and W. B. Head (1961), Relationships between porosity, media size, and sorting coefficients of synthetic sands, *J. Sediment. Petrol.*, *31*, 467–470.
- Sahimi, M. (1995), *Flow and Transport in Porous Media and Fractured Rock*, 482 pp., VCH, New York.
- Sen, P. N., C. Scala, and M. H. Cohen (1981), Self similar model for sedimentary rocks with application to the dielectric constant of fused glass beads, *Geophysics*, *46*, 781–795, doi:10.1190/1.1441215.
- Sok, R. M., M. A. Knackstedt, A. P. Sheppard, W. V. Pinczewski, W. B. Lindquist, and A. Venkatarangan (2002), Direct and stochastic generation of network models from tomographic images: Effect of topology on residual saturation, *Transp. Porous Media*, *46*, 345–371, doi:10.1023/A:1015034924371.
- Spanne, P., J. F. Thovert, C. J. Jacquin, W. B. Lindquist, K. W. Jones, and P. M. Adler (1994), Synchrotron computed microtomography of porous media: Topology and transport, *Phys. Rev. Lett.*, *73*, 2001–2004, doi:10.1103/PhysRevLett.73.2001.
- Stauffer, D., and A. Aharony (1992), *Introduction to Percolation Theory*, 2nd ed., 192 pp., Taylor and Francis, London.
- Thovert, J. F., F. Yousefian, P. Spanne, C. G. Jacquin, and P. M. Adler (2001), Grain reconstruction of porous media: Application to a low-porosity Fontainebleau sandstone, *Phys. Rev. E*, *63*, 061307, doi:10.1103/PhysRevE.63.061307.
- Walsh, J. B., and W. F. Brace (1984), The effect of pressure on porosity and the transport properties of rock, *J. Geophys. Res.*, *89*, 9425–9431, doi:10.1029/JB089iB11p09425.
- Zhan, X., L. M. Schwartz, M. N. Toksöz, W. C. Smith, and F. D. Morgan (2010), Pore-scale modeling of electrical and fluid transport in Berea sandstone, *Geophysics*, *75*, F135–F142, doi:10.1190/1.3463704.

Y. Bernabé, Earth, Atmospheric and Planetary Sciences Department, Massachusetts Institute of Technology, Cambridge, MA 02139, USA.

M. Li and Y. B. Tang, State Key Laboratory of Oil and Gas Reservoir Geology and Exploitation, Southwest Petroleum University, Chengdu 610500, China.

A. Mainault and M. Zamora, Institut de Physique du Globe de Paris, Sorbonne Paris Cité, Université Paris Diderot, F-75005 Paris, France.